

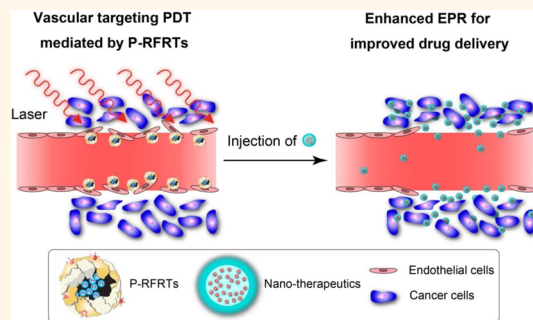
Tumor Vasculature Targeted Photodynamic Therapy for Enhanced Delivery of Nanoparticles

Zipeng Zhen,^{†,§} Wei Tang,^{†,§} Yen-Jun Chuang,[‡] Trevor Todd,[†] Weizhong Zhang,[†] Xin Lin,[§] Gang Niu,[§] Gang Liu,^{||} Lianchun Wang,[‡] Zhengwei Pan,[‡] Xiaoyuan Chen,[§] and Jin Xie^{†,‡,*}

[†]Department of Chemistry, University of Georgia, Athens, Georgia 30602, United States, [‡]Department of Physics, University of Georgia, Athens, Georgia 30602, United States, [§]National Institute of Biomedical Imaging and Bioengineering (NIBIB), National Institutes of Health (NIH), Bethesda, Maryland 20852, United States,

^{||}Key Laboratory of Molecular Vaccinology and Molecular Diagnostics & Center for Molecular Imaging and Translational Medicine, School of Public Health, Xiamen University, Xiamen, 361102, China, [‡]Department of Biochemistry and Complex Carbohydrate Research Center (CCRC), University of Georgia, Athens, Georgia 30602, United States, and [#]Bio-Imaging Research Center (BIRC), University of Georgia, Athens, Georgia 30602, United States. ^{*These authors contributed equally to this work.}

ABSTRACT Delivery of nanoparticle drugs to tumors relies heavily on the enhanced permeability and retention (EPR) effect. While many consider the effect to be equally effective on all tumors, it varies drastically among the tumors' origins, stages, and organs, owing much to differences in vessel leakiness. Suboptimal EPR effect represents a major problem in the translation of nanomedicine to the clinic. In the present study, we introduce a photodynamic therapy (PDT)-based EPR enhancement technology. The method uses RGD-modified ferritin (RFRT) as "smart" carriers that site-specifically deliver $^1\text{O}_2$ to the tumor endothelium. The photodynamic stimulus can cause permeabilized tumor vessels that facilitate extravasation of nanoparticles at the sites. The method has proven to be safe, selective, and effective. Increased tumor uptake was observed with a wide range of nanoparticles by as much as 20.08-fold. It is expected that the methodology can find wide applications in the area of nanomedicine.



KEYWORDS: photodynamic therapy · EPR · ferritin · nanoparticles · drug delivery · integrin $\alpha_v\beta_3$

Nanoparticle-based drugs are emerging as an important class of therapeutics. At least nine nanoparticle drugs have received regulatory approval for the treatment and diagnosis of various indications.^{1,2} These include Doxil and Abraxane, both of which have entered mainstream clinical cancer management. Unlike conventional small-molecule chemotherapeutics, nanoparticle- or macromolecule-based drugs can selectively egress at leaky tumor vasculatures and remain in the tumor interstitium for an extended period of time. This mechanism, referred to as the enhanced permeability and retention, or EPR, effect, has served as a foundation for modern nanomedicine.^{3,4} Compared to the extensive and intensive research in this area, however, the translation of nanomedicine into the clinic has been slow, if not disappointing. This has led to recent retrospections, concerning that the EPR effect

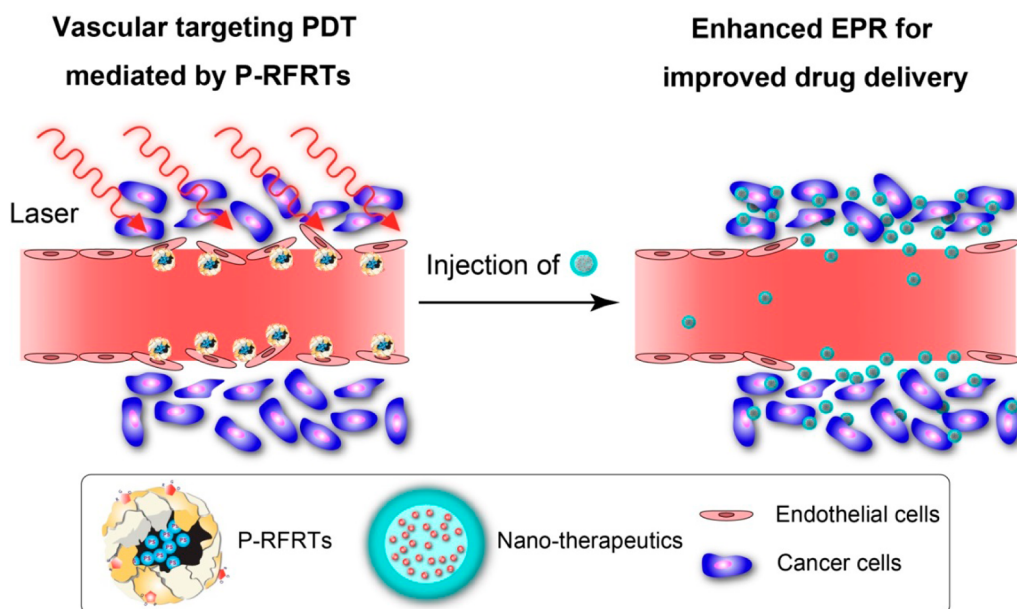
may have been overestimated.⁴ Despite relative leakiness compared to normal vessels, the endothelial lining can remain a barrier to the delivery of nanoparticles to tumors. This hindrance varies among tumors of different origins, stages, and organs and may affect the treatment efficacy significantly. One indication is the frequently reduced treatment efficacy of nanoparticle drugs in the clinic compared to animal studies. One primary reason is that many preclinical investigations are conducted in subcutaneous tumor models, where tumors develop within a short period of time and in a position of a rich vascular network.² Many of these tumors have high levels of EPR that is not often observed in human patients.^{2,4} This situation underscores the significance of an EPR enhancement technology that can enhance tumor endothelium leakiness.⁴ Prior work in this respect has focused on chemical-based vascular mediators such as

* Address correspondence to jinjie@uga.edu.

Received for review February 25, 2014 and accepted May 7, 2014.

Published online May 07, 2014
10.1021/nn501134q

© 2014 American Chemical Society



Scheme 1. Working mechanism of P-RFRT-mediated PDT for enhanced delivery of nanoparticles to tumors. P-RFRTs are first injected and locate to tumor endothelium through RGD–integrin interactions. With irradiation at an appropriate irradiance, the procedure generates ${}^1\text{O}_2$, which acts on the endothelium. This leads to enlarged or newly formed endothelial gaps. Due to the increased leakiness, nanoparticles injected subsequently will extravasate and accumulate more efficiently at tumors.

nitroglycerin, ACE inhibitors, and PGE1 agonists. With these, a 2–3-fold increase of EPR effect in tumors can be achieved.⁵ This approach, however, may potentially cause side-effects to normal vasculatures and organs due to the systemic nature.

We herein report a photodynamic therapy (PDT)-based method that can selectively increase vessel leakiness in tumors, linked to enhanced EPR effect. PDT is a clinically approved therapeutic procedure that consists of three components: photosensitizers, light, and oxygen.^{6,7} Photosensitizers, while not toxic individually, can be activated by light of a specific wavelength. This causes energy transfer to nearby oxygen molecules that produces cytotoxic ${}^1\text{O}_2$. A common target in conventional PDT is the tumor vasculature.^{6,8} In the clinic, vasculature PDT is achieved by controlling the time interval between photosensitizer injection and illumination, the so-called drug–light interval. Lacking selectivity, this toxicity acts on both endothelial and luminal targets (e.g., red blood cells/platelets), causing massive destruction that includes vessel collapse and thrombus formation.⁶ Our hypothesis is that with selective delivery and appropriate irradiation, PDT can be managed to increase vessel permeability but not induce occlusion. Particles injected subsequently can benefit from the permeabilized endothelium for enhanced accumulation in tumors.

To achieve this goal, we used RGD-modified ferritin (RFRT) as photosensitized carriers. Ferritin is a nontoxic protein nanocage found in most living organisms, including human beings. In nature, the main function of ferritin is to load Fe. When grown artificially (by *E. coli*) with no iron feeding, however, ferritins afford a

central cavity, which, as shown in our recent studies, can encapsulate metals or metal-containing compounds with high efficiency.^{9–11} In particular, ZnF₁₆Pc, a potent PS (λ_{max} : 671 nm; Φ_{Δ} : 0.85 in tetrahydrofuran¹²), can be encapsulated into RFRTs by up to 60 wt %.¹¹ Due to multiple RGD ligands (24-mer) on the surface, RFRTs have a strong binding affinity toward integrin $\alpha_v\beta_3$,¹³ which is overexpressed on neoplastic endothelial cells.^{14,15} Our studies showed that after systemic administration ZnF₁₆Pc-loaded RFRTs (P-RFRTs) can locate to the endothelium of neoplastic vessels via RGD–integrin interactions.¹¹ This, in combination with photoirradiation at a low irradiance, can permeabilize vasculature in tumors (Scheme 1). The notion was confirmed in 4T1, U87MG, MDA-MB-435S, and PC-3 tumor xenograft models using albumins, quantum dots, and iron oxide nanoparticles (IONPs). The treatment can increase tumor accumulation of nanoparticles by as much as 20.08-fold, while causing no adverse effects to normal tissues. Using Doxil as a representative nanoparticle drug, we also studied the impact of the procedure on cancer treatment. While exerting little cytotoxic power itself, P-RFRT-mediated PDT can improve the treatment efficacy of Doxil by 75.3%, which was attributed to the enhanced EPR effect. All these observations suggest P-RFRT-mediated PDT as a safe, selective, and effective means for enhanced nanoparticle delivery.

RESULTS AND DISCUSSIONS

Tumor Targeting with P-RFRTs. The preparation of RFRTs and how to load ZnF₁₆Pc onto RFRTs have been reported previously.¹¹ A formulation with a ZnF₁₆Pc

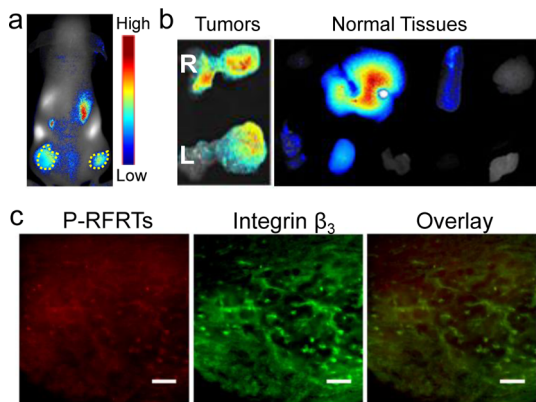


Figure 1. Tumor targeting of P-RFRTs. (a) *In vivo* imaging studies ($n = 5$). P-RFRTs were labeled with IRDye800 and were iv administered into bilateral 4T1 tumor models. Fluorescence imaging performed at 24 h showed selective accumulation of P-RFRTs in both tumors (circled by yellow dashed lines). (b) *Ex vivo* imaging with tumors as well as normal tissues. The normal tissues were arranged in the following order: first row, heart, liver, spleen, and skin; second row, intestine, kidney, muscle, and brain. (c) Immunofluorescence staining with tumor samples. Tumor vessels were stained by anti-integrin β_3 antibodies. Overall good correlation was found between P-RFRTs and positive integrin β_3 staining, suggesting that the tumor targeting was mainly mediated by RGD–integrin interactions. Scale bars, 100 μm .

loading rate of ~ 41.2 wt % was used in the current studies. Despite the heavy loading, the size of the resulting ZnF_{16}Pc -loaded RFRTs, or P-RFRTs, is relatively small (~ 18.6 nm).¹¹ It has also been observed in previous studies that P-RFRTs are stable in physiological environments and are not toxic in the dark.¹¹

We first studied tumor targeting efficiency of P-RFRTs in bilateral 4T1 (murine breast cancer) tumor xenograft models ($n = 5$). To facilitate the tracking, we labeled P-RFRTs with IRDye800 (ex/em: 780/800 nm, Licor). These labeled P-RFRTs (0.75 mg $\text{ZnF}_{16}\text{Pc}/\text{kg}$) were intravenously (iv) injected, and their migration was studied by fluorescence imaging on a Maestro II scanner. Accumulation of signals in both left and right tumors was observed (Figure 1a and Supporting Information Figure S1). At 24 h, the average tumor-to-normal (T/N) tissue ratio was 94.51 (97.52 ± 10.60) and 91.50 ± 13.00 for left and right tumors, respectively; Figure 1a and b), indicating high tumor selectivity. It was observed that, in addition to tumors, P-RFRTs also accumulated in the liver, spleen, and intestines. This distribution pattern is typical for nanoparticles of similar sizes. There was also a certain level of kidney accumulation. This was attributed to the moderate expression of integrin $\alpha_v\beta_3$ in the kidneys.¹⁶ The accumulation of P-RFRTs in these organs, however, causes few side-effects¹¹ due to the relatively deep positions. Immunofluorescence staining on tumor sections revealed overall good correlation between the P-RFRTs' distribution and positive integrin β_3 staining, suggesting that the targeting was mainly mediated by

RGD–integrin interactions (Figure 1c). Notably, 4T1 cells express a relatively low level of integrin $\alpha_v\beta_3$ on the surface. Many of the P-RFRTs, therefore, were positioned on tumor vessels instead of tumor cells at 24 h (Figure 1c).

Evaluating the EPR Enhancement Effect with Albumins.

Using human serum albumins (HSA) as drug mimics, we then studied the impact of P-RFRT-mediated PDT on the EPR effect. With a molecular weight of $\sim 65\,000$ and a diameter of ~ 7 nm, HSA is a good representative of macromolecules or small nanoparticles.¹⁷ The study was composed of two steps. In the first step, P-RFRTs (0.75 mg $\text{ZnF}_{16}\text{Pc}/\text{kg}$) were iv administered ($n = 3$), followed by photoirradiation by a 671 nm laser at 24 h. The laser was delivered in the form of a 1 cm beam that covers the right-side tumor of an animal. The left-side tumors were not irradiated and served as controls. An irradiance of 14 mW/cm^2 (for 30 min) was applied, which was much lower than the power used in conventional PDT ($50\text{--}300\text{ mW/cm}^2$).¹⁸ In the second step, IRDye800-labeled HSA (1 mg/kg) was iv injected 5 min after the end of the laser irradiation. The animals were then subjected to fluorescence imaging, and the accumulation of probes in the left and right tumors was compared.

At all the time points examined, there was a significantly higher uptake of probes in the right-side tumors (Figure 2a). By region-of-interest (ROI) analysis, we quantified and compared the relative increase of tumor uptake (RIU), which is the ratio of fluorescence readings between the right and left tumors. At 1, 4, and 24 h, RIU was 1.88 ± 0.29 , 2.23 ± 0.34 , and 2.96 ± 0.27 , respectively. After 24 h of imaging, the animals were euthanized and the tumors were harvested. The *ex vivo* imaging with tumors revealed a similar level of difference in uptake between the irradiated and unirradiated tumors (Figure 2a). The enhanced tumor uptake by PDT was further assessed by microscopy studies (Figure 2c). Interestingly, in addition to overall increased uptake, there is also a change in the distribution pattern of the albumins: In unirradiated tumors, the albumins were found only in the tumors' peripheries; in irradiated tumors, on the other hand, albumins penetrated much deeper into the masses.

To confirm the enhancement effect, we also conducted similar studies in 4T1 tumor models that bear one tumor each. We treated the tumors by the same injection and irradiation procedures (14 mW/cm^2 for 30 min at 24 h after P-RFRT injection), followed by albumin administration (IRDye800 labeled, 1 mg/kg). In the two control groups, animals received P-RFRTs but no irradiation, or irradiation only, before albumin injections. Compared to the controls, increased tumor accumulation was observed in the PDT-treated animals (Figure 2b). At 24 h, an increased uptake of 2.41 ± 0.39 -fold was observed between the irradiated and unirradiated groups. This amplitude of increase is

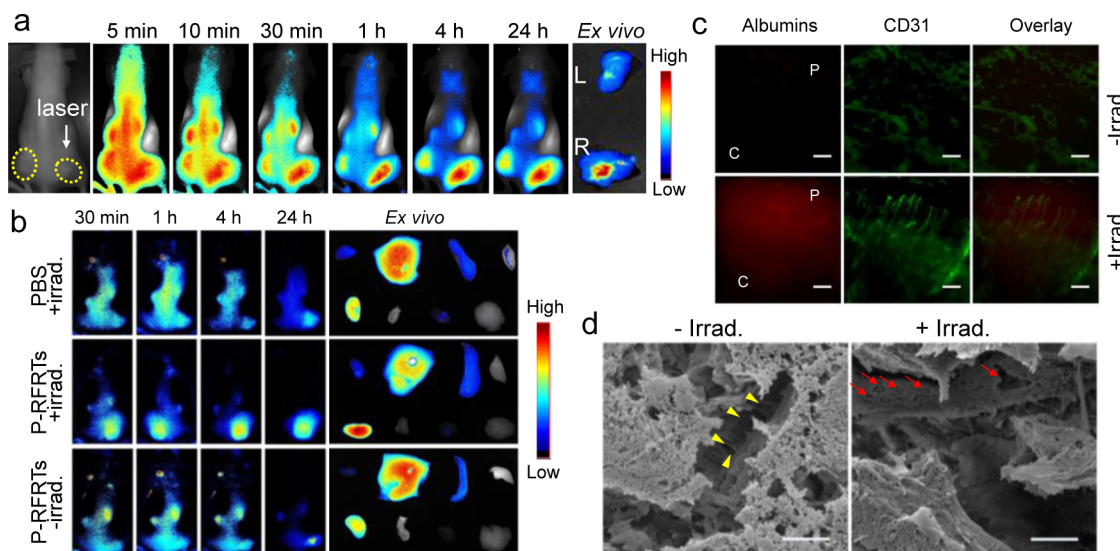


Figure 2. Study of the EPR enhancement effect with albumins. (a) PDT-induced EPR enhancement. The study was performed in bilateral 4T1 tumor models. P-RFRTs were iv injected first. A 671 nm laser was applied to the right-side tumors 24 h after injection of P-RFRTs. IRDye800-labeled HSA was injected 5 min after the end of the irradiation. Significantly enhanced tumor accumulation (by 2.96 ± 0.27 -fold at 24 h, $p < 0.05$) was observed in irradiated tumors over unirradiated ones. *Ex vivo* imaging with dissected tumors showed a similar level of increase in albumin uptake. (b) EPR enhancement effect, investigated in 4T1 tumor models that bear one tumor each. Animals were divided into three groups ($n = 3$) and were treated with P-RFRTs plus irradiation, PBS plus irradiation, and P-RFRTs only, respectively. Compared to the two control groups, animals receiving the P-RFRTs and irradiation combination showed significantly increased tumor uptake of HSA. On the other hand, the distribution of albumins in normal tissues was comparable among the three groups. For *ex vivo* imaging, the tissues were arranged in the following order: first row, heart, liver, spleen, and skin; second row, kidney, intestine, muscle, and brain. (c) Immunofluorescence staining. Enhanced tumor accumulation was observed in the group that had undergone PDT (P-RFRTs + irradiation) before the HSA injection. It is also noted that albumins penetrated much deeper into the tumors after the PDT modulation. “p” and “c” indicate the peripheral and central regions of a tumor, respectively. Scale bars, 100 μm . (d) SEM study on tumor sections. Compared to the unirradiated tumors, more and larger fenestrae were found on the endothelial walls of the irradiated tumors (highlighted by red arrows). In addition, compared to the unirradiated tumors, where vessels were enriched with bridge- and tunnel-like structures (pointed out by yellow arrows), the PDT-treated tumors showed a much smoother wall surface. Scale bars, 2.5 μm .

comparable to that observed in bilateral tumor models. As a matter of fact, comparable RIU values between the two sets of studies were observed at all time points (Supporting Information Figure S2). The harvested tumors and normal tissues were then subjected to *ex vivo* imaging (Figure 2b). There was no significant difference in albumin accumulation in normal tissues among the three groups. This suggests that the PDT treatment is highly selective. Aside from increasing tumor uptake, it has little impact on the delivery of albumins to other organs.

To elucidate the mechanism behind the uptake increase, in a separate study, we sacrificed animals 5 min after the end of irradiation (without injection of albumins) and harvested the tumors for scanning electron microscopy (SEM) analysis. Compared to the unirradiated tumors, we observed many more large fenestrae on the endothelial walls of the irradiated ones (Figure 2d, highlighted by red arrows). This is attributed to PDT-induced contraction and rounding of tumor endothelial cells that enlarged endothelial gaps or formed new ones.¹⁹ The yielded vessels are thus more permeable, which is believed to be the primary cause behind the enhanced tumor uptake. Interestingly, changes were also found on the luminal

microstructures after the PDT: Without irradiation, the lumen of vessels was enriched with branched lining cells, which formed extensive bridges and tunnels (Figure 2d, highlighted by yellow arrows). These features are commonplace in poorly developed tumor vessels, as observed by others.²⁰ In contrast, tumors that had undergone irradiation displayed much smoother vessel surface (Figure 2d), indicating a possible plumbing function of the PDT procedure. This hypothesis is corroborated by immunofluorescence microscopy on tumors before as well as 5 min and 24 h after the PDT (Supporting Information, Figure S4). Untreated tumors featured irregular and convoluted vessels, which correlate with the SEM observations. After the PDT treatment, however, the blood vessels become more regular and ordered, probably more so at 5 min (Supporting Information, Figure S3). This indicates a possible vessel normalization effect by the PDT, although the impact is temporary. Both the vessel dredging and vessel normalization are attributed to PDT, but the exact mechanism is unknown at this stage. It could be that the $^1\text{O}_2$ acted on the branched lining cells, forcing their contraction into the endothelium or even being uprooted from it. These lead to a lesser degree of complexity of the microstructures.

Nonetheless, bridged and tunneled microstructures in blood vessels can pose great geometric resistance to the blood flow and, in turn, lead to elevated interstitial fluid pressure (IFP).²¹ Commonly observed in solid tumors, elevated IFP is a major barrier to deliver drugs to the masses, especially to the central regions. It is more an issue for delivery of macromolecules/nanoparticles, which, due to their relatively large size, depend heavily on convection rather than diffusion for extravasation.^{22,23} A modulation that can clear and normalize the vessels is therefore of great value in improving the delivery. This hypothesis seems to be supported by microscopic imaging studies, which found in PDT-treated tumors not only increased overall accumulation but also improved dispersion of albumins (Figure 2b).

The tumor samples were also subjected to TUNEL assays, which evaluate the toxicity caused by PDT. Interestingly, few cell deaths were detected in the PDT-treated tumors (Supporting Information Figure S5). This suggests that despite the vascular effects the PDT induced, its toxicity to the surroundings is minimal. This is attributable to the low fluence and fluence-rate used and, also, to the accurate endothelium targeting. In combination, the $^1\text{O}_2$ generated acts as a gentle, local cleaning of the vessels, thereby avoiding the extensive vessel occlusion and destruction that is often observed in conventional PDT.

Fluence Dependence of the EPR Enhancement. The impact of PDT is often dependent on fluence and irradiance. It is postulated, therefore, that the EPR effect is also fluence dependent. To examine this, we repeated the preceding study with bilateral 4T1 tumor models but varied the irradiance (the illumination time was fixed at 30 min). RIU values from different irradiation conditions were then assessed and compared. At 3 mW/cm^2 , there was almost no enhancement effect, showing an RIU value of 1.03 ± 0.24 at 24 h (Figure 3a). Increasing the irradiance to 8 mW/cm^2 led to enhanced tumor uptake (1.43 ± 0.38 at 24 h), but the amplitude was smaller than that at 14 mW/cm^2 (2.96 ± 0.27). Further increasing irradiance beyond 14 mW/cm^2 to 22 mW/cm^2 did not enhance the tumor uptake accordingly, showing an RIU value of 1.89 ± 0.36 at 24 h (Figure 3a). The difference in tumor uptake was better illustrated by immunofluorescence staining. Compared to the control and other illumination conditions, the 14 mW/cm^2 group manifested the most prominent probe accumulation and dispersion (Figure 3b). These results show that increased irradiance and fluence is not always beneficial to the EPR enhancement. While too low an irradiation dose can be insufficient to induce vessel permeabilization, a too high irradiation dose can be overkill, possibly causing partial or complete occlusion of the vessel, which adversely affects the nanoparticle delivery.

EPR Enhancement in Different Tumor Models. Using the same injection and irradiation plans, we also evaluated

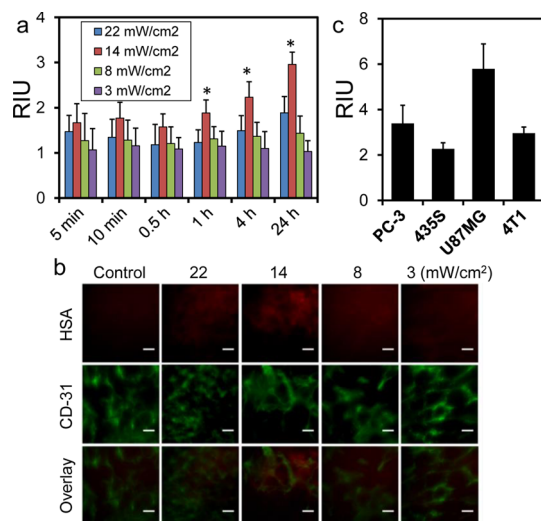


Figure 3. The EPR enhancement is irradiance dependent. (a) Histogram comparison of relatively increased tumor uptake under irradiation at different irradiances. The data were derived from ROI analyses on the *in vivo* imaging results. The highest RIU values were observed at 14 mW/cm^2 for all time points. * indicates $p < 0.05$. (b) Immunofluorescence staining results. Many more albumins (IRDye800, red) were found outside blood vessels (marked by CD31 staining, green) after the PDT, suggesting an enhanced EPR effect. The most prominent accumulation and dispersion were observed at 14 mW/cm^2 . Scale bars, 100 μm . (c) EPR enhancement effect in different tumors ($n = 3$). The results were based on comparison of 24 h tumor accumulation between irradiated and unirradiated tumors. A similar or even superior EPR enhancement effect was observed in PC-3, MDA-MB-435S, and U87MG tumor models.

the EPR enhancement effect in other tumor models. These include PC-3 (humane prostate cancer), MDA-MB-435S (human melanoma), and U87MG (human glioblastoma) tumor-bearing mice. In every model, we observed enhanced accumulation of albumins in tumors after the PDT treatment (Figure 3c and Supporting Information Figures S6–S8). Specifically, 24 h RIU values were 3.39 ± 0.80 , 2.27 ± 0.27 , and 5.79 ± 1.10 , respectively, for PC-3, MDA-MB-435S, and U87MG tumors. Similarly, the PDT treatment caused little change in distribution of albumins in normal tissues (Supporting Information Figure S9). Notably, integrin $\alpha_v\beta_3$ is expressed moderately or abundantly on the surface of PC-3 (integrin $\alpha_v\beta_3^+$), MDA-MB-435S (integrin $\alpha_v\beta_3^{++}$), and U87MG (integrin $\alpha_v\beta_3^{+++}$) cells. Hence, some or a large amount of injected P-RFRTs located to cancer cells in these models. The fact that a comparable or even superior enhancement effect was observed in these models suggests that the PDT effects on cancer cells do not affect the EPR enhancement, at least not adversely.

EPR Enhancement for QDs and IONPs. We next examined whether the method applies to particles with a larger size. This was first investigated with quantum dots (QDs, from Invitrogen, ex/em: 405–665/705 nm), which have a diameter of ~ 50 nm (Supporting Information Figure S10). The study was performed on

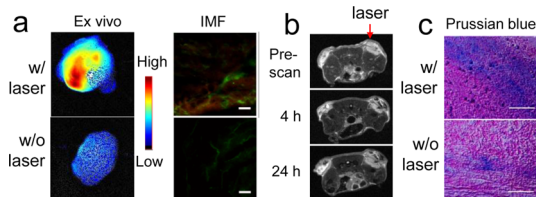


Figure 4. EPR enhancement with nanoparticles. (a) EPR enhancement effect with QDs. The study was performed in bilateral 4T1 tumor models. QDs were injected 5 min after the end of P-RFRT-mediated PDT, which was applied only to the left-side tumors. *Ex vivo* imaging was performed on dissected tumors 24 h after the QD injection. Compared to unirradiated tumors, irradiated tumors showed a 20.8-fold increase in tumor uptake (by ROI analysis). This was further confirmed by immunofluorescence (IMF) staining. Green, CD31, marks blood vessels; red, QDs. Scale bars, 100 μ m. (b) EPR enhancement effect with IONPs ($n = 3$). The study was performed in bilateral 4T1 tumor models. IONPs were injected 5 min after the end of P-RFRT-mediated PDT, which was applied only to the right-side tumors. MR images were taken before and 4 and 24 h after the injection of IONPs. More significant signal drop was observed in the right-side, irradiated tumors. (c) Prussian blue staining on tumor samples from b. Correlated with the *in vivo* observations, more iron deposits were found in irradiated tumors. Scale bars, 100 μ m.

bilateral 4T1 tumor models. Similarly, QDs were injected after P-RFRT-mediated PDT (30 pmol/mouse, $n = 3$). The contralateral tumor receiving no photoirradiation served as the control. After 24 h, we sacrificed the animals and dissected the tumors for comparison by *ex vivo* imaging (Figure 4a, Supporting Information Figure S11). ROI analyses on *ex vivo* imaging with dissected tumors revealed an RIU of 20.08 ± 1.28 between irradiated and unirradiated tumors. This significant increase in the EPR enhancement over that found with albumins could be due to a number of factors, which include the difference in particle dimensions. Due to the larger size of QDs, the endothelial lining represents a more difficult barrier for them than for albumins. Therefore, the PDT treatment, which lowers the threshold, works more effectively on QDs to improve their extravasation at the tumors. The difference may have been further augmented by the fact that large nanoparticles are less mobile. That is, compared to albumins, QDs have a higher tendency to stay at the tumor interstitial space after the extravasation. This was supported by immunofluorescence staining, which found a large amount of QDs accumulated just outside the blood vessels (Figure 4a). In contrast, albumins were disseminated much deeper from the vessels (Figure 2c).

The PDT-based method also applies to iron oxide nanoparticles. In a separate study, ~40 nm IONPs (core size ~15 nm, Ocean Nanotech) as model nanoparticles were injected into bilateral 4T1 tumor models after the PDT ($n = 3$). A commonly used MRI contrast probe, IONPs shorten T_2 relaxation times of nearby protons, causing regional signal drop on T_2 -weighted MR maps. Compared to the unirradiated side, many more signal

voids were observed in the irradiated tumors, indicating an enhanced tumor accumulation (Figure 4b). The result was further validated by Prussian blue staining, which found more iron deposits in tumors that had undergone irradiation (Figure 4c).

EPR Enhancement for Improving Tumor Therapy with Doxil.

With the encouraging imaging results, we then moved forward to therapy studies. This was evaluated in 4T1 xenograft tumor models (bearing one tumor each). Doxil, a liposome-based doxorubicin drug, was used as a nanoparticle therapeutic. Specifically, animals were injected with P-RFRTs first (0.75 mg/kg), followed by irradiation at 24 h (14 mW/cm² for 30 min). Right after the irradiation, Doxil (10 mg/kg) was iv administered ($n = 5$). Several control groups were also studied. These include animals receiving P-RFRTs and Doxil but no irradiation, P-RFRTs and irradiation but no Doxil, Doxil and irradiation, Doxil only, and PBS only ($n = 5$).

The group that received PDT only (P-RFRTs+Irrad.) showed a similar tumor growth rate to animals receiving only PBS (Figure 5a). This indicates that PDT alone caused few therapeutic effects. The data correlate well with the observations from TUNEL assays (Supporting Information Figure S5), which found little toxicity of PDT at this low irradiance. Animals treated with P-RFRTs + Doxil, Doxil + irradiation, and Doxil only showed comparable but mediocre tumor suppression. On day 12, tumor growth inhibition (TGI) rates were computed to be 39.4%, 56.7%, and 49.0% for these three groups, respectively (Figure 5a). In contrast, significantly improved tumor growth inhibition was observed in animals receiving both PDT and Doxil (P-RFRTs+Irrad.+Doxil). The combination almost completely arrested tumor growth in the first week, including two animals showing tumor shrinkage. On day 12, a TGI of 85.9% was observed. This represents an increased treatment efficacy by 75.3% compared to Doxil alone (Figure 5a). Given that the PDT individually has no direct therapy contribution, the improvement must have been due to the enhanced EPR caused by the PDT.

After the therapy studies, we sacrificed the animals. The tumors were dissected and compared both visually (Figure 5b) and by weight (Supporting Information Figure S12). The results corroborate well with the measurements in Figure 5a. We also performed TUNEL assays on the tumor tissues taken 24 h after treatment (Figure 5d). A significantly higher level of cell death was observed in the group receiving the PDT and Doxil combination. Otherwise, there was no sign of additional toxicity induced by the PDT (Supporting Information Figure S13). These include no additional heart toxicity, which is commonly associated with Doxil-based treatments (Supporting Information Figure S14). Also, there was no significant difference of body weights between the treatment group and other groups receiving Doxil (Figure 5c). All these observations suggest

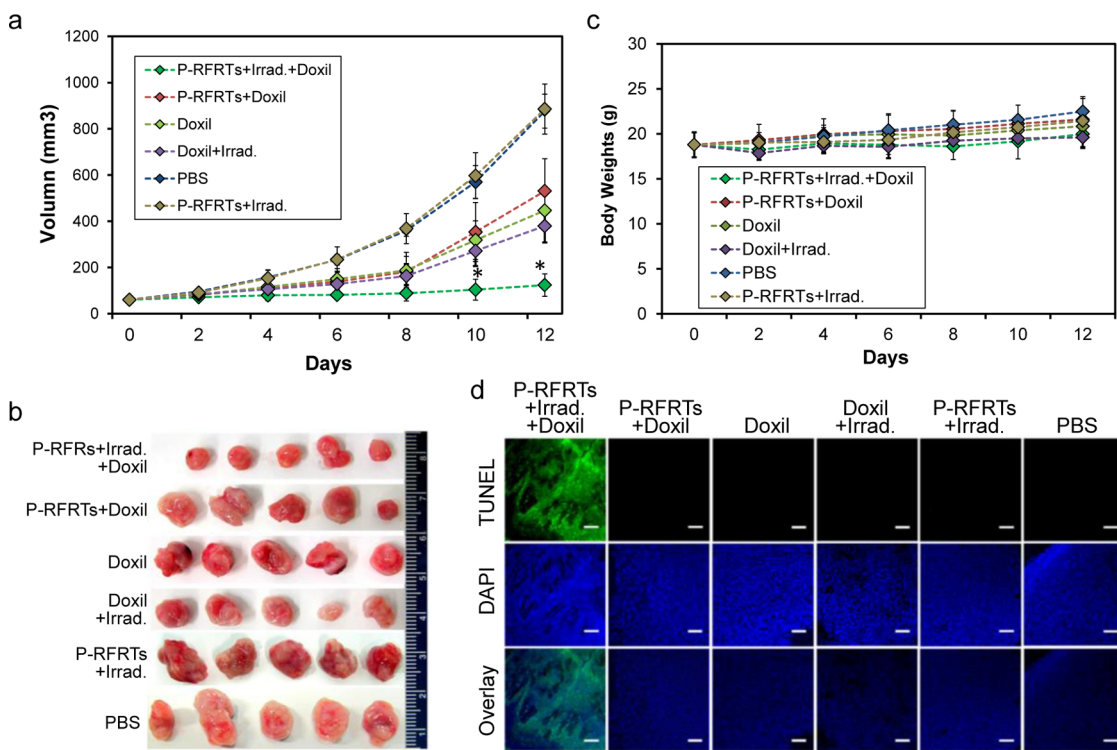


Figure 5. ERP enhancement for improved tumor therapy. (a) Therapy results. The study was performed in 4T1 tumor models ($n = 5$). Doxil was injected 5 min after the end of P-RFRT-mediated PDT. Control groups include animals receiving P-RFRTs and Doxil but no irradiation, Doxil only, irradiation only, P-RFRTs and irradiation but no Doxil, and PBS only. Compared to the control groups, animals receiving the PDT and Doxil combination showed much more significant tumor growth suppression, manifesting a TGI of 85.9% on day 12. * $p < 0.05$. (b) Photographs of dissected tumors from a. (c) Body weight growth curves. Compared to other groups receiving Doxil, the combination therapy caused no additional weight loss. (d) TUNEL assays on tumor sections. A high level of cell death was observed only in animals treated with the combination therapy. Green, TUNEL. Blue, DAPI. Scale bars, 100 μ m.

that the PDT modulation is highly selective and of minimal contralateral damage.

CONCLUSION

Nanotherapeutics, whether taking an active or passive targeting approach, relies heavily on the EPR effect to achieve tumor accumulation. Even if engineered to be long-circulating and tumor selective, without efficient extravasation at the tumor sites, nanoparticle drugs will end up accumulating in normal organs and cause serious side-effects. P-RFRT-mediated PDT represents a novel and safe means that can augment the EPR effect without affecting normal tissues. The technology employs the inherent selective nature of PDT, the site-specific delivery capacity of RFRTs, and an optimized irradiance. In combination, the method induces selective and controlled PDT stimuli to the tumor endothelium, leading to increased vessel leakiness while not blocking the blood flow. The approach has proven to be effective in different tumor models to facilitate delivery of nanoparticles to tumors. In particular, it was observed in 4T1 tumor-bearing mice that the EPR enhancement effect can translate to enhanced treatment efficacy of Doxil. Future investigations, however, are needed to assess the methodology in tumors of different origins and stages and to optimize the

modulation to gain maximum therapeutic benefits and potentially reduced systematic toxicity.

PDT-induced vessel permeabilization has been observed previously.^{24,25} The effect, however, is usually accompanied and often overwhelmed by other vascular effects such as vessel collapse and occlusion.²⁵ Recently, Snyder *et al.* observed that HPPH-based PDT at low fluence rates can be employed to improve delivery of nanoparticles to tumors.²³ More recently, Wang *et al.* reported that low-dose PDT with verteporfin can lead to increased tumor uptake of Liporubicin.²⁶ These observations corroborate with ours in that the irradiation dose is important to EPR enhancement and should be carefully gauged for the optimal effect. In the previous investigations, vascular targeting was achieved by controlling the time interval between photosensitizer injection and illumination, the so-called drug–light interval. Illuminating at an early time point confines the damage mostly within the vasculature, and that at a late time point mostly on cancer cells.¹² This passive targeting approach has been commonly used in the clinic for therapy purposes. It, however, is often associated with side-effects that may limit its uses for EPR enhancement. Most commonly used photosensitizers, such as verteporfin, HPPH, Photofrin, chlorin e6, and 5-aminolaevulinic acid, show low

tumor-to-normal-tissue (T/N) ratios (around or less than 2).^{13–15} In theory, PDT damage can be controlled by photoirradiation that is only given to areas of interest. In reality, however, collateral damage to surrounding normal tissues is often observed.²⁷ Also, poor T/N selectivity leads to photosensitivity due to high accumulation of photosensitizers in the skin and eyes. For instance, Photofrin-treated patients are required to stay out of sunlight for at least 4 weeks,¹⁷ and Foscavir-injected patients may experience photosensitivity to even interior lighting for at least 1 week post-treatment.¹⁷ These side-effects can significantly affect the life quality of patients and are not acceptable when PDT is used as an adjuvant modality whose main purpose is to enhance chemotherapy. For this application, P-RFRT-mediated PDT is a better approach given the high photosensitizer payload, great tumor selectivity, and minimal skin toxicity.¹¹

As mentioned before, the surface of ferritins can be easily modified. In addition to RGD, other types of vasculature targeting motifs, for instance F3 peptide²⁸

and sialyl Lewis^X²⁹ can be introduced onto the ferritin surface. Moreover, a very recent study by Sano *et al.* showed that with proper photoirradiation IR700-conjugated panitumumab can kill perivascular cancer cells and, in turn, enhance the tumor EPR effect.³⁰ It will be interesting to develop ferritin derivatives presenting different targeting motifs on the surface and evaluate them for either therapy or EPR enhancement purposes.

The technology also benefits the delivery of macromolecules to tumors, as demonstrated in the case of albumins. Macromolecule therapeutics, in particular monoclonal antibody-based drugs, have achieved rapid advances in the past decade and are emerging as a new category of therapeutics, with 13 antibodies already receiving regulatory approval.³¹ This trend is further fueled by the recent progress on developing antibody–drug conjugates (ADCs), which utilizes antibodies as vehicles to transport cytotoxic agents to tumors in a site-specific manner.³² It is highly expected that our technology as an adjuvant can find wide applications in the delivery of these drugs as well.

MATERIALS AND METHODS

Cell Culture. 4T1 (murine breast cancer), U87MG (human glioblastoma), PC-3 (human prostate cancer), and MDA-MB-435S (human melanoma) cell lines were purchased from ATCC. 4T1 and PC-3 cells were grown in RMPI 1640 medium supplemented with 10% fetal bovine serum (FBS) and 1% penicillin and streptomycin (MediaTech, USA). U87MG cells were grown in DMEM medium containing 10% FBS, 1% nonessential amino acids, and 1% penicillin and streptomycin. These three cell lines were incubated humidly under 37 °C and 5% CO₂. MDA-MB-435S cells were grown in the same medium as 4T1 and PC-3 but were incubated without CO₂.

Ferritin Purification and ZnF₁₆Pc Loading. The protocols for producing RFRTs and loading ZnF₁₆Pc onto them have been published.¹¹ For IRDye800 labeling, P-RFRTs were incubated with IRDye800 for 30 min and purified through a NAP-5 column to remove uncoupled dye molecules. A starting ratio of 2:1 (IRDye800 to RFRTs) was used. The coupling efficiency was assessed spectroscopically by comparing with a predetermined standard curve (by monitoring absorbance at 780 nm). It was determined that the final conjugates have on average one IRDye800 per particle.

Animal Models. Animal models were established by subcutaneous injection of ~10⁶ cancer cells (4T1, PC-3, MDA-MB-435S, and U87MG) to either one side or both sides of the hindlimbs of 5–6-week athymic nude mice.³³ For 4T1 tumor models, the *in vivo* studies were conducted 1 week after the inoculation when the tumors reached a size of ~100 mm³. For PC-3, MDA-MB-435S, and U87MG tumor models, the *in vivo* studies were conducted 3 weeks after the inoculation, when the tumors reached a size of ~100 mm³. All the animal studies were performed according to a protocol approved by the Institutional Animal Care and Use Committee (IACUC) of University of Georgia.

Tumor Targeting with P-RFRTs. For tumor targeting studies, IRDye800-labeled P-RFRTs (0.75 mg ZnF₁₆Pc/kg) were iv injected to bilateral 4T1 tumor models (*n* = 5). Whole-body fluorescence images were acquired on a Maestro II imaging system (PerkinElmer) using an NIR emission filter (750–940 nm) up to 24 h postinjection. After the 24 h imaging, the animals were euthanized. The tumors as well as major organs were harvested for *ex vivo* imaging and histology studies.

EPR Enhancement Studies by Fluorescence Imaging. For EPR enhancement studies, the animals were iv injected with P-RFRTs (0.75 mg ZnF₁₆Pc/kg) first (*n* = 3). For bilateral tumor models, the right-side tumors were irradiated by a 671 nm laser (~1 cm diameter beam) for 30 min. The left-side tumors were shielded by aluminum foil and served as the control. For single-tumor models, two control groups (*n* = 3) received P-RFRTs but not irradiation and PBS only. The irradiances were measured by a laser power meter (FieldMax II, Coherent) and were varied (3, 8, 14, and 22 mW/cm²). IRDye800-labeled HSA (0.5 mg/kg) was administered 5 min after the end of the 30 min irradiation. The animals were then subjected to fluorescence imaging on Maestro II using an NIR emission filter (750–940 nm). After 24 h of imaging, the animals were sacrificed. The tumors as well as major organs were harvested for *ex vivo* imaging and histology studies. Uptake in a given organ was quantified by ROI analyses on both *in vivo* and *ex vivo* imaging results using the software provided by the vendor. The studies with QDs (Invitrogen, ex/em: 405–665/705 nm) were conducted in bilateral 4T1 tumor models (injected at 30 pmol per mouse). The procedures were similar to those with HSA except that a different emission filter (640–820 nm) was selected.

EPR Enhancement Studies with IONPs. The studies were conducted in bilateral 4T1 tumor models. The animals were iv injected with P-RFRTs (0.75 mg ZnF₁₆Pc/kg) first (*n* = 3). The right-side tumors were irradiated 24 h later by a 671 nm laser (14 mW/cm², over a ~1 cm diameter beam) for 30 min. The left-side tumors were shielded by aluminum foil and served as the control. Five minutes after the end of the irradiation, IONPs (Ocean Nanotech) at a dose of 10 mg Fe/kg were iv injected. T2-weighted FSE images were acquired on a 7 T Varian small animal MRI system before and 4 and 24 h after the particle injection. The following parameters were used for the scans: TR = 2.5 s; TE = 48 ms; ETL = 8; FOV = 40² mm²; matrix size = 256²; 13 axial slices with 1 mm slice thickness. After the 24 h scan, the mice were sacrificed. The tumors were collected and snap-frozen for Prussian blue staining.

In Vivo Therapy Studies. The therapy studies were performed in 4T1 tumor models (one tumor each animal). Briefly, 30 4–6-week female nude mice were subcutaneously injected with ~10⁶ 4T1 cells to the right hindlimb. The 30 mice were randomly divided into 6 groups, 5 mice each group. The study started 5 days after the inoculation (average tumor size of 50.68 ± 18.79 mm³).

For the treatment group, the animals were iv injected with P-RFRTs first (0.75 mg ZnF₁₆Pc/kg). The tumors were irradiated 24 h later by a 671 nm laser (14 mW/cm², over a ~1 cm diameter beam) for 30 min. Doxil was iv injected 5 min after the end of the irradiation at a dose of 10 mg/kg. The five control groups received (1) P-RFRTs and Doxil, but no irradiation; (2) Doxil only; (3) PBS and irradiation, no P-RFRTs and Doxil; (4) PBS only; and (5) P-RFRTs and irradiation, no Doxil. The tumors sizes and body weights were measured every other day. Tumor sizes were measured by a caliper and computed following the following formula: size (mm³) = length (mm) × width (mm)²/2.

Immunofluorescence Staining. The cryogenic slides were fixed with cold acetone for 30 min, washed by running water for 5 min, and blocked by 10% goat serum for 1 h. Anti-integrin β_3 (ab75872, Abcam) or phycoerythrin-labeled anti-CD31 (ab25644, Abcam) antibodies were incubated with the slides at 4 °C overnight. Cy5.5-labeled secondary antibodies (ab6564, Abcam) were then added and incubated with the slides at 37 °C for 1 h. After gently rinsing with PBS, the slides were mounted and ready for microscopic imaging. TUENL assays were performed by following a protocol provided by the vendor (FITC-labeled POD, GenScript).

Scanning Electron Microscopy. Tumor blocks were cut into 10 μm slices. The slices were mounted on coverslips and fixed by 0.5% paraformaldehyde at 4 °C for 48 h. For dehydration, ethanol of gradient concentrations (25%, 50%, 75%, 90%, and 100%) was applied to the slices at room temperature, 30 min for each step. These slides were then sputter-coated with a gold/palladium mix after critical point dried in a SAM-DRI-790 CPD³⁴ and then analyzed using a field emission gun SEM (FEI INSPECT F FEG-SEM).

Hematoxylin and Eosin Staining. H&E staining was performed according to a protocol provided by the vendor (BBC Biochemical). Briefly, 8 μm cryogenic slides were prepared and fixed with 10% formalin for about 30 min at room temperature. After washing with running water for 5 min, the slides were treated with gradient concentrations of alcohol (100, 95, and 70%), each for 20 s. The hematoxylin staining was performed for about 3 min, and the slides were washed with water for 1 min. The eosin staining was performed for about 1 min. The slides were washed, treated with xylene, and mounted with Canada balsam. The images were acquired on a Nikon Eclipse 90i microscope.

Statistical Methods. Quantitative data were expressed as mean \pm SD. Means were compared using Student's t test. *p* values < 0.05 were considered statistically significant.

Conflict of Interest: The authors declare no competing financial interest.

Acknowledgment. J.X. was support by an NCI/NIH R00 grant (5R00CA153772). X.C. was supported by the Intramural Research Program of NIBIB, NIH. Z.W.P. acknowledges financial support from the National Science Foundation (CAREER DMR-0955908). L.C.W. acknowledges the funding from NIH R01HL093339 and RR005351/GM103390.

Supporting Information Available: Additional information as noted in the text. This material is available free of charge via the Internet at <http://pubs.acs.org>.

REFERENCES AND NOTES

- Wang, A. Z.; Langer, R.; Farokhzad, O. C. Nanoparticle Delivery of Cancer Drugs. *Annu. Rev. Med.* **2012**, *63*, 185–198.
- Taurin, S.; Nehoff, H.; Greish, K. Anticancer Nanomedicine and Tumor Vascular Permeability: Where Is the Missing Link?. *J. Controlled Release* **2012**, *164*, 265–275.
- Maeda, H. Vascular Permeability in Cancer and Infection as Related to Macromolecular Drug Delivery, with Emphasis on the EPR Effect for Tumor-Selective Drug Targeting. *Proc. Jpn. Acad., Ser. B* **2012**, *88*, 53–71.
- Prabhakar, U.; Maeda, H.; Jain, R. K.; Sevick-Muraca, E. M.; Zamboni, W.; Farokhzad, O. C.; Barry, S. T.; Gabizon, A.; Grodzinski, P.; Blakey, D. C. Challenges and Key Considerations of the Enhanced Permeability and Retention Effect for Nanomedicine Drug Delivery in Oncology. *Cancer Res.* **2013**, *73*, 2412–2417.
- Maeda, H.; Nakamura, H.; Fang, J. The EPR Effect for Macromolecular Drug Delivery to Solid Tumors: Improvement of Tumor Uptake, Lowering of Systemic Toxicity, and Distinct Tumor Imaging *In Vivo*. *Adv. Drug Delivery Rev.* **2013**, *65*, 71–79.
- Dolmans, D. E. J. G. J.; Fukumura, D.; Jain, R. K. Photodynamic Therapy for Cancer. *Nat. Rev. Cancer* **2003**, *3*, 380–387.
- Fisher, A. M.; Murphree, A. L.; Gomer, C. J. Clinical and Preclinical Photodynamic Therapy. *Lasers Surg. Med.* **1995**, *17*, 2–31.
- Nishiyama, N.; Morimoto, Y.; Jang, W. D.; Kataoka, K. Design and Development of Dendrimer Photosensitizer-Incorporated Polymeric Micelles for Enhanced Photodynamic Therapy. *Adv. Drug Delivery Rev.* **2009**, *61*, 327–338.
- Zhen, Z. P.; Tang, W.; Chen, H. M.; Lin, X.; Todd, T.; Wang, G.; Cowger, T.; Chen, X. Y.; Xie, J. RGD-Modified Apoferritin Nanoparticles for Efficient Drug Delivery to Tumors. *ACS Nano* **2013**, *7*, 4830–4837.
- Todd, T. J.; Zhen, Z. P.; Xie, J. Ferritin Nanocages: Great Potential as Clinically Translatable Drug Delivery Vehicles?. *Nanomedicine (London, U.K.)* **2013**, *8*, 1555–1557.
- Zhen, Z. P.; Tang, W.; Guo, C. L.; Chen, H. M.; Lin, X.; Liu, G.; Fei, B. W.; Chen, X. Y.; Xu, B. Q.; Xie, J. Ferritin Nanocages To Encapsulate and Deliver Photosensitizers for Efficient Photodynamic Therapy against Cancer. *ACS Nano* **2013**, *7*, 6988–6996.
- Garcia, A. M.; Alarcon, E.; Munoz, M.; Scaino, J. C.; Edwards, A. M.; Lissi, E. Photophysical Behaviour and Photodynamic Activity of Zinc Phthalocyanines Associated to Liposomes. *Photochem. Photobiol. Sci.* **2011**, *10*, 507–514.
- Lin, X.; Xie, J.; Niu, G.; Zhang, F.; Gao, H.; Yang, M.; Quan, Q.; Aronova, M. A.; Zhang, G.; Lee, S.; et al. Chimeric Ferritin Nanocages for Multiple Function Loading and Multimodal Imaging. *Nano Lett.* **2011**, *11*, 814–819.
- Tan, M.; Lu, Z. R. Integrin Targeted MR Imaging. *Theranostics* **2011**, *1*, 83–101.
- Zhang, Y.; Yang, Y.; Cai, W. Multimodality Imaging of Integrin Alpha(v)Beta(3) Expression. *Theranostics* **2011**, *1*, 135–148.
- Li, Z. B.; Cai, W.; Cao, Q.; Chen, K.; Wu, Z.; He, L.; Chen, X. (64)Cu-Labeled Tetrameric and Octameric RGD Peptides for Small-Animal PET of Tumor Alpha(v)Beta(3) Integrin Expression. *J. Nucl. Med.* **2007**, *48*, 1162–1171.
- Kong, G.; Braun, R. D.; Dewhirst, M. W. Hyperthermia Enables Tumor-Specific Nanoparticle Delivery: Effect of Particle Size. *Cancer Res.* **2000**, *60*, 4440–4445.
- Dougherty, T. J.; Gomer, C. J.; Henderson, B. W.; Jori, G.; Kessel, D.; Korbelik, M.; Moan, J.; Peng, Q. Photodynamic Therapy. *J. Natl. Cancer Inst.* **1998**, *90*, 889–905.
- Kanthou, C.; Tozer, G. M. The Tumor Vascular Targeting Agent Combretastatin A-4-Phosphate Induces Reorganization of the Actin Cytoskeleton and Early Membrane Blebbing in Human Endothelial Cells. *Blood* **2002**, *99*, 2060–2069.
- Hashizume, H.; Baluk, P.; Morikawa, S.; McLean, J. W.; Thurston, G.; Roberge, S.; Jain, R. K.; McDonald, D. M. Openings between Defective Endothelial Cells Explain Tumor Vessel Leaking. *Am. J. Pathol.* **2000**, *156*, 1363–1380.
- Less, J. R.; Posner, M. C.; Skalak, T. C.; Wolmark, N.; Jain, R. K. Geometric Resistance and Microvascular Network Architecture of Human Colorectal Carcinoma. *Microcirculation* **1997**, *4*, 25–33.
- Heldin, C. H.; Rubin, K.; Pietras, K.; Ostman, A. High Interstitial Fluid Pressure - An Obstacle in Cancer Therapy. *Nat. Rev. Cancer* **2004**, *4*, 806–813.
- Snyder, J. W.; Greco, W. R.; Bellnier, D. A.; Vaughan, L.; Henderson, B. W. Photodynamic Therapy: A Means to Enhanced Drug Delivery to Tumors. *Cancer Res.* **2003**, *63*, 8126–8131.
- Debefve, E.; Mithieux, F.; Perentes, J. Y.; Wang, Y. B.; Cheng, C.; Schaefer, S. C.; Ruffieux, C.; Ballini, J. P.; Gonzalez, M.

- van den Bergh, H.; *et al.* Leukocyte-Endothelial Cell Interaction Is Necessary for Photodynamic Therapy Induced Vascular Permeabilization. *Lasers Surg. Med.* **2011**, *43*, 696–704.
25. Chen, B.; Pogue, B. W.; Luna, J. M.; Hardman, R. L.; Hoopes, P. J.; Hasan, T. Tumor Vascular Permeabilization by Vascular-Targeting Photosensitization: Effects, Mechanism, and Therapeutic Implications. *Clin. Cancer Res.* **2006**, *12*, 917–923.
26. Wang, Y. B.; Gonzalez, M.; Cheng, C.; Haouala, A.; Krueger, T.; Peters, S.; Decosterd, L. A.; van den Bergh, H.; Perentes, J. Y.; Ris, H. B.; *et al.* Photodynamic Induced Uptake of Liposomal Doxorubicin to Rat Lung Tumors Parallels Tumor Vascular Density. *Lasers Surg. Med.* **2012**, *44*, 318–324.
27. Allison, R. R.; Downie, G. H.; Cuenca, R.; Hu, X. H.; Childs, C. J. H.; Sibata, C. H. Photosensitizers in Clinical PDT. *Photodiagn. Photodyn.* **2004**, *1*, 27–42.
28. Winer, I.; Wang, S. Y.; Lee, Y. E. K.; Fan, W. Z.; Gong, Y. S.; Burgos-Ojeda, D.; Spahlinger, G.; Kopelman, R.; Buckanovich, R. J. F3-Targeted Cisplatin-Hydrogel Nanoparticles as an Effective Therapeutic That Targets Both Murine and Human Ovarian Tumor Endothelial Cells *in Vivo*. *Cancer Res.* **2010**, *70*, 8674–8683.
29. Farr, T. D.; Lai, C. H.; Grunstein, D.; Orts-Gil, G.; Wang, C. C.; Boehm-Sturm, P.; Seeger, P. H.; Harms, C. Imaging Early Endothelial Inflammation Following Stroke by Core Shell Silica Superparamagnetic Glyconanoparticles That Target Selectin. *Nano Lett.* **2014**, *14*, 2130–2134.
30. Sano, K.; Nakajima, T.; Choyke, P. L.; Kobayashi, H. Markedly Enhanced Permeability and Retention Effects Induced by Photo-Immunotherapy of Tumors. *ACS Nano* **2013**, *7*, 717–724.
31. Sliwkowski, M. X.; Mellman, I. Antibody Therapeutics in Cancer. *Science* **2013**, *341*, 1192–1198.
32. Kovtun, Y. V.; Goldmacher, V. S. Cell Killing by Antibody-Drug Conjugates. *Cancer Lett.* **2007**, *255*, 232–240.
33. Edwards, B. K.; Brown, M. L.; Wingo, P. A.; Howe, H. L.; Ward, E.; Ries, L. A.; Schrag, D.; Jamison, P. M.; Jemal, A.; Wu, X. C.; *et al.* Annual Report to the Nation on the Status of Cancer, 1975–2002, Featuring Population-Based Trends in Cancer Treatment. *J. Natl. Cancer Inst.* **2005**, *97*, 1407–1427.
34. Moore-Scott, B. A.; Gordon, J.; Blackburn, C. C.; Condie, B. G.; Manley, N. R. New Serum-Free *in Vitro* Culture Technique for Midgestation Mouse Embryos. *Genesis* **2003**, *35*, 164–168.